sciendo
ISSN 1335-8871
MEASUREMENT SCIENCE REVIEW
Journal homepage: https://content.sciendo.com

Experimental Validation of a High-Speed Tracked Vehicle Powertrain Simulation Model

Luka Ponorac[1*], Ivan Blagojević[2]

[1]*AMSS - Center for motor vehicles Ltd., Kneginje Zorke 58, 11000, Belgrade, Serbia, luka.ponorac@amss-cmv.co.rs*
[2]*Department of Motor Vehicles, Faculty of Mechanical Engineering, University of Belgrade, Kraljice Marije 16, 11000, Belgrade, Serbia, iblagojevic@mas.bg.ac.rs*

Abstract: High-speed tracked vehicles have complex powertrains that, in addition to power transfer and transformation, also perform the functions of vehicle steering and braking systems, as well as power supply system for various subsystems on the vehicle. Analyzing the power balance of a tracked vehicle, especially in specific moving scenarios such as the turning process, is of great importance for understanding the power requirements and workload of the powertrain components and their optimization. A simulation model was developed, based on the construction parameters of an experimentally tested high-speed tracked vehicle to reduce the time and material resources required for experimental testing. Both the simulation and experimental tests were conducted using the same input parameters and driving conditions for different vehicle turning scenarios. Simulation and experimental test results are compared to verify the accuracy of the simulation model. The analysis of the obtained results shows that the average value of the relative rpm error is about 5%, the average value of the relative torque error is about 7%, while the average value of the relative power error is about 6.5%.

Keywords: High-speed tracked vehicle, powertrain, workload analyses, vehicle experimental testing, vehicle dynamics.

1. INTRODUCTION

The development process of a new vehicle, as well as the modernization of an existing one, often requires a significant amount of time and resources for project development and testing, especially when complex experimental testing is required. When it comes to the development of a new powertrain (or subsystems of similar significance) of a high-speed tracked vehicle, experimental field tests are almost inevitable due to the extreme working conditions that often result in unpredictable workloads on the drive components [1], [2]. Given the fact that high-speed tracked vehicles are most commonly used as combat vehicles, the subsystem components must have a high level of reliability and be thoroughly tested and verified. In order to optimize the construction of the powertrain components, the experimental tests must be repeated often. However, using only the "trial and error" method in the development of tracked vehicles has proven to be expensive. Wong and Preston-Thomas noticed this and were among the first to use the Computer Simulation Model as part of the vehicle development process [3]. In order to reduce the number of experimental tests and thus reduce the overall resources required for the vehicle/subsystem development, it has become common practice to develop a credible simulation model of the subject vehicle that is verified by the results of the experimental field tests [4], [5], [6]. The main purpose of the simulation model is to predict and quantify the impact of the proposed solutions before the final design and testing [7].

Developing a realistic simulation model of a high-speed tracked vehicle is not an easy task, given the fact that the full model of these vehicles would consist of many components and subsystems, which would unnecessarily complicate the simulation process and make it unreasonably long [8]. This is why the simulation model should be simplified as much as possible, but not oversimplified to a point where important vehicle subsystem parameters are neglected.

There are several approaches to developing a high-speed tracked vehicle simulation model. One of the most popular methods is to develop a mathematical model of the vehicle and specific vehicle subsystems in a software such as MATLAB and its subprogram Simulink [9]. Janarthanan et al. used MATLAB Simulink to develop a simulation model of a high-speed tracked vehicle to analyze the dynamic load on the vehicle and compare the results with the results of experimental tests. They found that the simulation model has an advantage over experimental tests, especially when it comes to time and cost reduction [10], [11], [18].

Another popular vehicle development method is to develop a 3D vehicle model based on the known vehicle and subsystem construction, working principles, materials and other parameters, using CAD software. The 3D model of the

DOI: 10.2478/msr-2023-0025

Corresponding author: luka.ponorac@amss-cmv.co.rs (L. Ponorac)

vehicle is then analyzed in software specifically designed for various numerical analyses [12], [13]. According to Madsen et al., the most popular approaches for developing a vehicle model are Super-Element Models and the Multibody approach [14], [15]. In general, researchers claim that the most efficient approach for developing the high-speed tracked vehicle simulation model is the Multibody approach [16], [17].

In the paper presented, the powertrain subsystem is developed in detail to analyze the dynamic workloads during different movement conditions. The vehicle model contains the model of the forces resisting the vehicle movement in order to simulate the experimental test conditions as accurately as possible.

The aim of this paper is to validate the high-speed tracked vehicle mathematical model in order to use it for the future development and modernization of the subject vehicle. The assessment and validation of the model accuracy is done by comparing it with the experimental test results of the real vehicle.

2. SUBJECT & METHODS

The method used in this paper is based on the comparison and analysis of simulation models and experimental tests, in a similar manner as in [19]. The first step of building a simulation model is to develop an accurate vehicle model based on known vehicle construction parameters. The next step is to develop a model of the propulsion and resisting forces acting on the vehicle during different moving scenarios. The most specific and demanding movement scenario for a high-speed tracked vehicle is the turning process, where additional power is used to provide the different track rewinding speed and to overcome the turning resistance forces [20], [21], [22].

A. Subject vehicle

The high-speed tracked vehicle used for simulation model development and experimental testing has a mechanical powertrain with two power flows, as shown in Fig. 1.

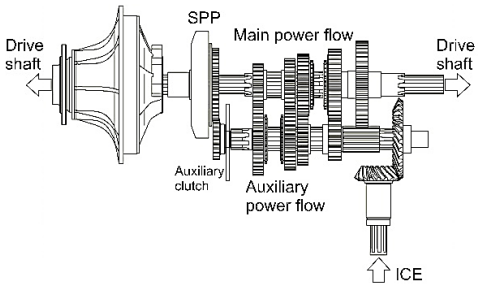

Fig. 1. Subject vehicle powertrain.

The main power flow is always activated and transfers the power parameters from the IC engine through the gearbox to the tracks. The auxiliary power flow is activated when the vehicle enters the turning process, through friction clutches or brakes. Part of the engine power is transferred through the auxiliary power flow to the summarizing planetary gear set (SPP, Fig. 1) of the inner track, where it is combined with the power from the main flow, as shown in Fig. 2. This results in a reduction in the output angular velocity of the planetary gear set, and thus a reduction in the rewinding speed of the inner track. The inner track is the track with the lower velocity around which the vehicle is turning [23].

When the turning mechanism friction clutch is activated, the vehicle turns with a defined calculated radius. This state of the turning process is specific because of the circulating power, referred to as recuperation power, which appears in the powertrain. This circulating power has a positive effect on the vehicle's power balance, as it supports the vehicle turning process by increasing the power in the outer track and thus reducing the power required from the IC engine, as shown in Fig. 2.

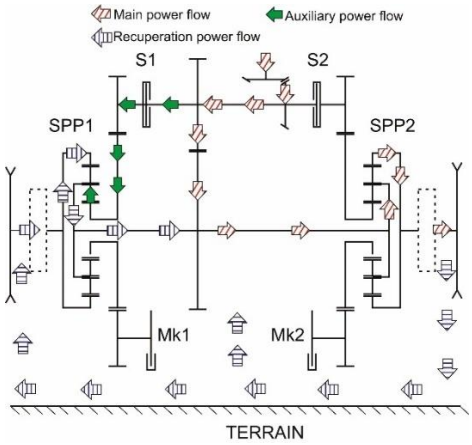

Fig. 2. Turning process powertrain kinematic scheme.

B. Simulation model

The vehicle simulation model is developed in MATLAB Simulink and combines mechanical components (IC engine, gearbox, brakes and clutches), physical components (forces representing moving resistance, friction, etc.), and Simulink components (signal converters, scopes, mathematical operation blocks).

The model is created from subsystems that are part of the vehicle powertrain system [24]. The model concept is shown in Fig. 3 and consists of the following subsystems:

- IC engine with main friction clutch
- Integrated powertrain subsystem
- Track subsystem
- Control block

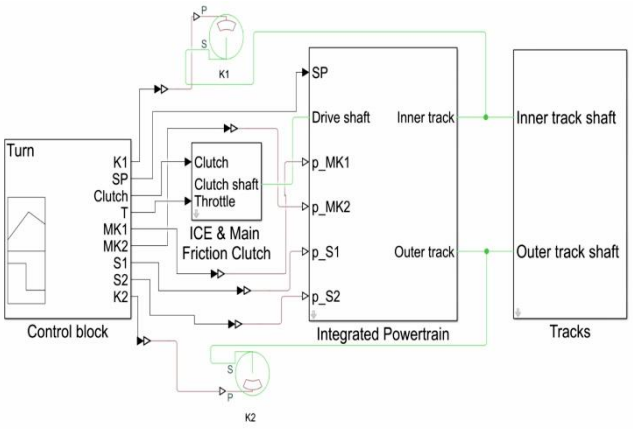

Fig. 3. Powertrain simulation model.

IC engine with main friction clutch subsystem

The IC engine with main friction clutch subsystem consists of three main blocks: IC engine, Clutch pedal, and Main friction clutch, as shown in Fig. 4.

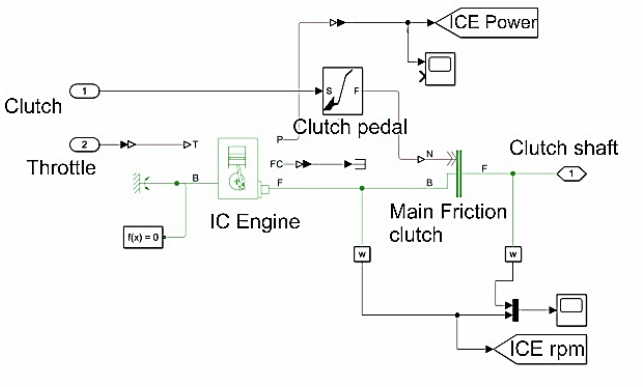

Fig. 4. ICE & main friction clutch subsystem.

The IC engine block represents the torque and angular velocity source for the powertrain, parametrized by speed-torque data collected during real ICE experimental testing, as shown in Fig. 5. Apart from basic speed-torque data, the ICE block is specified by engine type parameters (SI/CI), kinematic parameters (speed limits), and dynamic parameters (engine inertia).

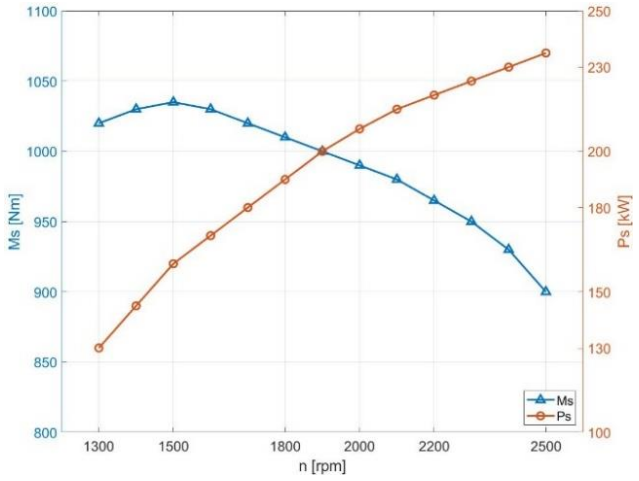

Fig. 5. ICE characteristic curve.

Engine torque and angular velocity, defined as ICE mechanical output signals, are transferred to the Integrated powertrain subsystem by means of the Main friction clutch block.

As in the experiment, the throttle input signal is one of the main simulation input data and represents the driver's demands. The throttle input signal lies between zero and one and specifies the torque demanded by the engine as a fraction of the maximum possible torque. If the engine speed falls below the Stall speed, the engine torque is blended to zero. The throttle position input signal is pre-set in the Control block, labeled T in Fig. 6, and corresponds to the throttle position information from the experimental test.

Fig. 6 shows all important simulation input data from the Control block, such as: SP-active gear ratio; Clutch-Main Friction Clutch activation pressure; Mk1, Mk2-Steering brakes activation pressure; S1, S2-auxiliary clutch activation pressure. These inputs correspond to the driver's actions via the commands during the experimental test.

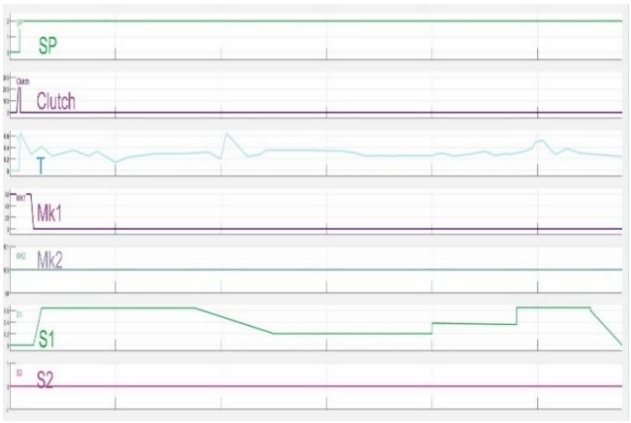

Fig. 6. Control block input signal.

The Main friction clutch block represents a model of the single-plate, dry friction clutch of the subject vehicle. The block consists of mechanical input and output ports and a physical port connected to the Clutch pedal block where the clutch activation/deactivation force is generated. The mechanical input port is connected to the ICE block, while the mechanical output port is connected to the Integrated powertrain subsystem. The Main friction clutch block is defined by the effective torque radius, kinetic and static friction coefficients, threshold force, and viscous losses (optional) so that the clutch model corresponds to the subject vehicle clutch parameters.

The Clutch pedal block represents the mechanical model of the clutch activation/deactivation mechanism by a system of levers shown in Fig. 7. The block receives the signal from the Control block representing the driver command (engagement/disengagement cycle), labeled Clutch in Fig. 6, and converts it into mechanical activation/deactivation force of the Main friction clutch.

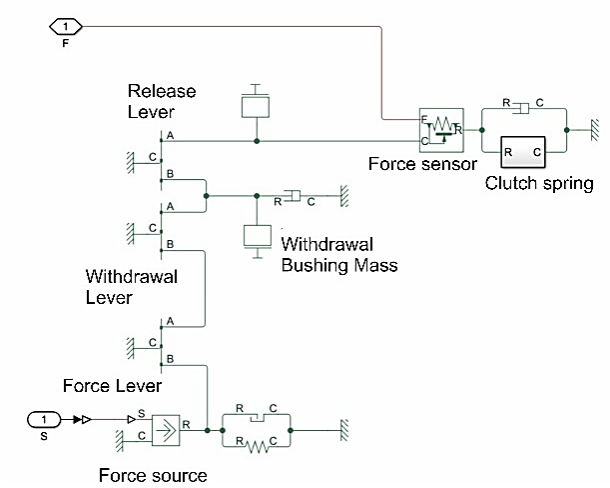

Fig. 7. Clutch command model.

Integrated powertrain subsystem

The subject vehicle powertrain is constructed in such a way that the gearbox and turning mechanisms are physically organized in a single housing called powertrain in block or integrated powertrain [25]. The simulation model of the integrated powertrain is designed in the same way as the real vehicle powertrain shown in Fig. 8.

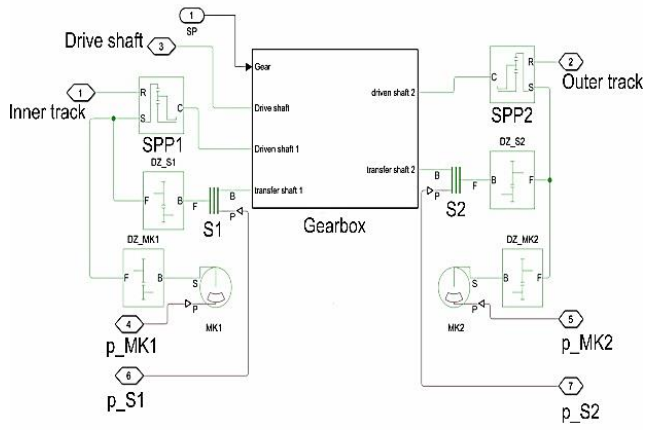

Fig. 8. Integrated powertrain subsystem.

The turning mechanism model consists of two summarizing planetary gear sets, labeled SPP1 and SPP2, and auxiliary engagement friction elements S1, S2, MK1, and MK2, all shown in Fig. 8.

The planetary gear sets SSP1 and SSP2 combine the power from the main and auxiliary power flows. Each planetary gear set model is connected to three mechanical signals: the main power flow (driven shaft), the auxiliary power flow (transfer shaft), and to the inner and outer track blocks representing the drive sprocket shafts and the tracks.

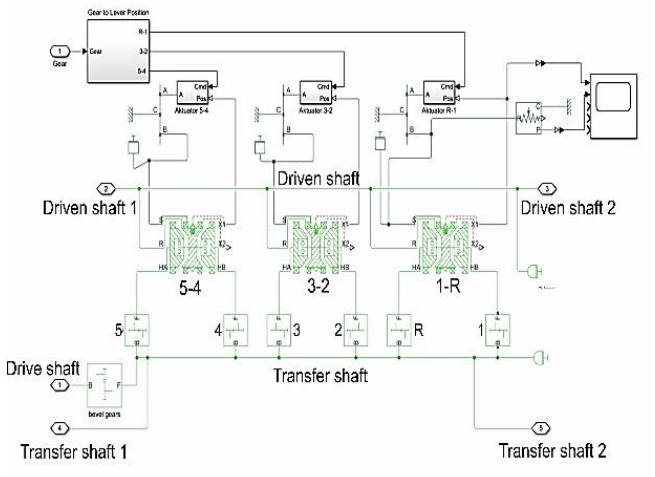

Fig. 9. Vehicle gearbox model.

Clutches S1 and S2 represent a model of real multi-lamellar auxiliary clutches modeled to simulate the transition states during the engagement/disengagement process of the auxiliary power flow. The clutch models are activated by means of the physical signals p_S1 and p_S2 of the Control block, shown as S1, S2 in Fig. 6.

The gearbox block represents the real manual, mechanical five-speed gearbox, as shown in Fig. 9. The block simulates the function of the real gearbox with the corresponding gear ratios and power loss in the gear pairs. The corresponding gear pairs are activated by synchronizer and actuator blocks connected to the Control block.

Kinematic and dynamic parameters are delivered from the Main Friction Clutch block to the gearbox Transfer shaft via the Drive shaft. From the Transfer shaft, power is then transferred to the driven shaft by activating one of the five forward gear ratios (1-5 blocks) or the reverse gear ratio (R-block). This represents the Main power flow. The gear blocks are activated by synchronizers labeled 5-4, 3-2, and 1-R. The synchronizers consist of double-sided dog and cone clutches. They have a mechanical translation port representing the ring shifter handle S and X1 and X2 ports representing the physical signal reporting the position of the synchronizer elements. Synchronizer assemblies are designed so that a gear signal (1-5) requested by the Control block activates the corresponding gear, shown as SP in Fig. 6.

When the auxiliary power flow is activated by engaging the S1 or S2 friction clutch, the power parameters are delivered from the transfer shaft to the corresponding summarizing planetary gear set SPP1 or SPP2. This is the auxiliary power flow. When the vehicle is turning, both the main and auxiliary power flows are active.

Track subsystem

The track subsystem consists of two track subsystems and the turning radius subsystem. The subsystem model is shown in Fig. 10.

Most simulation analyses are performed for the vehicle in turn, so the track subsystems are labeled Inner track and Outer track, referring to the track with the lower velocity, around which the vehicle turns, and the track with the higher velocity, which travels a longer distance.

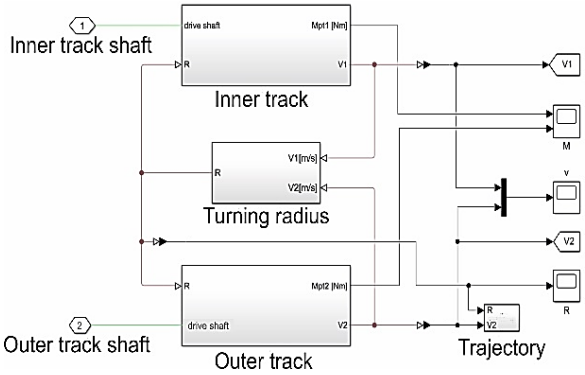

Fig. 10. Track subsystem model.

The subsystems are modeled as a combination of mechanical components (planetary gear set, torque and angular velocity sensors, shafts) and physical components that represent the forces acting on the vehicle and are explained later in the text. Mechanical parameters from the Track subsystem are converted into physical and mechanical signals that are sent to scopes and other blocks that provide visualization and manipulation with the measured parameters.

The turning radius subsystem represents the mathematical operation for determining the vehicle turning radius and trajectory based on the inner and outer track velocity. The construction of the block is shown in Fig. 11.

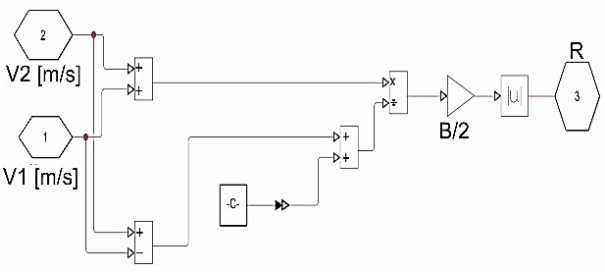

Fig. 11. Turning radius block.

The turning radius is determined by (1)

$$R = B/2 \cdot (V_2 + V_1)/(V_2 - V_1) \tag{1}$$

where:

- B - track width
- $V_2,\ V_1$ - outer and inner track velocities

The turning radius information signal is sent to both the inner and outer track subsystems, where it affects the turn resisting forces.

C. Vehicle dynamics model

The vehicle dynamics model represents the influence of vehicle movement scenarios on the propulsion and resisting forces acting on the vehicle. As mentioned earlier, tracked vehicles require more power during turning than during rectilinear movement to overcome the resisting forces resulting from the terrain structure and the nature of the track-surface contact [26].

The forces acting on the high-speed tracked vehicle during the turning process, are shown in Fig. 12

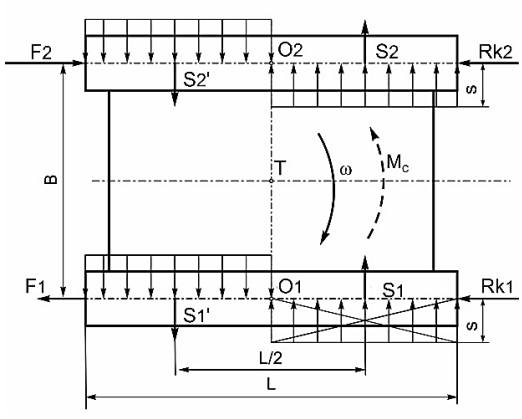

Fig. 12. Vehicle turning dynamics.

where:

- R_{k1}, R_{k2} - rectilinear moving resistance
- $S_1,\ S'_1, S_2, S'_2$ - lateral forces resulting from the lateral slip of the vehicle
- F_1, F_2 - propulsive forces
- M_C - turning resistance moment

Under realistic turning conditions, the turning process of the vehicle is always characterized by sliding and slipping of the tracks, resulting in lateral shift of the vehicle. The vehicle cuts and meshes the soil under the tracks, resulting in increased turning resistance [27], [28]. The specific lateral resistance acting on the vehicle is described in (2) and (3)

$$s = \mu \cdot G/2L \tag{2}$$

$$S_1 = S'_1 = S_2 = S'_2 = s \cdot L/2 = \mu \cdot G/4 \tag{3}$$

The coefficient μ is referred to in literature as the turning resistance coefficient empirically defined by (4)

$$\mu = \frac{\mu_{max}}{0.85+0.15\left(\frac{R}{B}+\frac{1}{2}\right)} \tag{4}$$

where:

- R - theoretical turning radius
- μ_{max} - value of coefficient μ at $R = B/2$

The turning resistance moment is then described as in (5)

$$M_C = (S_1 + S_2) \cdot L/2 = \mu GL/4 \tag{5}$$

When the vehicle is turning with a low velocity, the vehicle is subjected to rectilinear resisting forces described by (6)

$$R_{k1} = N_1 f =, R_{k2} = N_2 f = \frac{G}{2} f \tag{6}$$

Creating the movement balance equations in the theoretical rotation poles O1 and O2, Fig. 10, and solving (7) and (8)

$$\sum M_{O1} = F_2 \cdot B - R_{k2} \cdot B - M_C \tag{7}$$

$$\sum M_{O2} = F_1 \cdot B + R_{k1} \cdot B - M_C \tag{8}$$

The propulsion forces acting on the tracks can be described by (9)

$$F_2 = R_{k2} + \frac{M_C}{B},\ F_1 = -R_{k2} + \frac{M_C}{B} \tag{9}$$

By replacing the corresponding values from (5) and (6) into (9), the total vehicle propulsion forces are then defined as in (10)

$$F_2 = \frac{G}{2} f + \frac{\mu GL}{4B},\ F_1 = -\frac{G}{2} f + \frac{\mu GL}{4B} \tag{10}$$

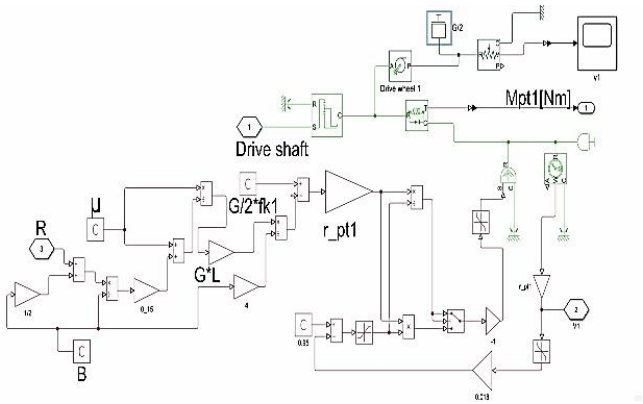

Fig. 13. Resisting forces model.

The dynamic forces acting on the vehicle are modeled as a physical signal in both the inner and outer track subsystems, as shown in Fig. 13. The physical signal representing the calculation of the turning resistance is converted into a mechanical signal (torque) and connected to the mechanical model of the drive wheels and drive shafts. The torque signal has the opposite direction of the drive shaft torque, so it represents the powertrain load due to the turning resistance.

D. Experimental test

To verify the created simulation model, experimental tests were performed with the subject vehicle in different turning scenarios. The turning scenarios were carefully recorded to use the same movement conditions to the simulation process, as far as possible.

The tests were conducted under dry conditions on levelled, soft clay and asphalt terrain. The vehicle is driven with different engine loads, gear changing, varying the position of the drive wheel, i.e. the auxiliary clutch activation pressure, and thus changing the turning radius.

Data acquisition

The measurement of the significant parameters is performed by wireless signal transfer and acquisition system, in a manner corresponding to methods in [29], [30]. Strain gauges with wireless signal transfer are attached to the integrated powertrain output shafts shown in Fig. 14 to measure powertrain output torque. Inductive gauges were used to measure the kinematic values of the powertrain (output angular velocities). The gauges are attached to the powertrain housing, while the reference measuring point is placed on the main brake disk.

Fig. 14. Position of the measuring equipment.

In order to record all the conditions of the turning scenario, a pressure gauge is installed in the auxiliary clutch hydraulic system, see Fig. 15. By measuring the auxiliary clutch activation pressure, precise information about the clutch working state is obtained, which gives us information about the vehicle moving regime.

Since the significant test parameters are measured on rotating powertrain components, the strain and angular velocity gauges used for the measurement have wireless data transmission. The QuantumX acquisition system is used for acquisition and processing of the measured signals, and the results are analyzed and displayed in the Catman software.

Fig. 15. Pressure gauge position.

Experimental test procedure

To compare the simulation and experimental test results, a specific part of the experimental test is selected and simulated in the simulation model.

The selected part of the experimental test includes such driving scenarios where the vehicle is driven in a certain gear, with a relatively constant input engine speed, and with the auxiliary friction clutch fully and partially engaged.

Vehicle trajectory is shown in Fig. 16. For the time interval $t \approx 0$ s - 35 s, the vehicle was turning with the auxiliary clutch fully engaged, making a full turn and starting a second one. The clutch is then partially disengaged in $t \approx 35$ s - 80 s, increasing the turning radius. From $t \approx 80$ s - 110 s, the clutch is again fully engaged, so that the turning radius decreases to the calculated radius and the vehicle makes another full turn and stops. The vehicle makes three full circle turns, the first and last with the auxiliary clutch fully engaged and the middle one with clutch slip because the auxiliary clutch is partially engaged.

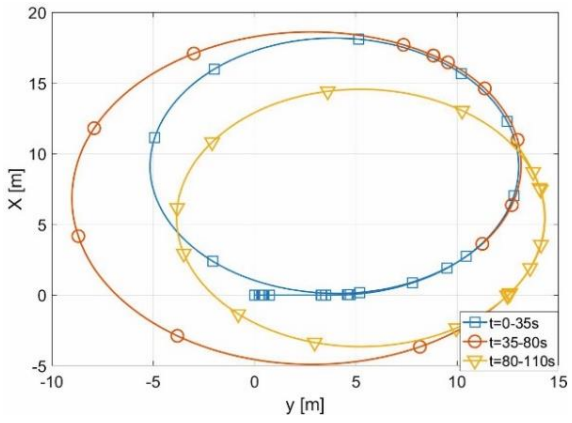

Fig. 16. Vehicle trajectory.

3. RESULTS

The input parameters of the experimental test (engine speed, auxiliary clutch activation pressure, active gear, brake activation pressure) are used as input parameters of the simulation to provide the same test conditions as much as possible. The simulation output values are compared with the experiment output values (powertrain output torque, angular velocity, and power) to validate the consistency of the simulation model with the real vehicle under the same conditions. The selected part of the whole experimental test

is where the subject vehicle was driven in second gear with a relatively constant input engine speed of about 850 rpm. Simulation input parameters are shown in Fig. 6.

Fig. 17 shows the auxiliary clutch engagement/disengagement during the turning process, which gives us information about the vehicle moving regime. The experimentally obtained pressure values are interpolated and used as input pressure values for the auxiliary clutch in the simulation model. The curves pS1 and pS1s represent the clutch activation pressure measured during the experimental tests and simulation, respectively.

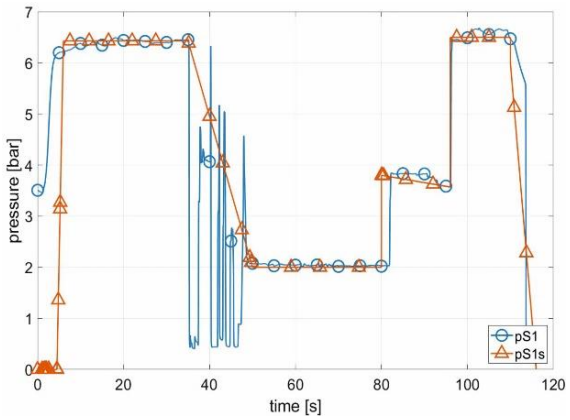

Fig. 17. Auxiliary clutch activation pressure-simulation vs experiment.

At the beginning of the turning process, the auxiliary clutch is fully engaged with a maximum activation pressure of $p \approx 6.5$ bar, as shown in Fig. 17. This means that the vehicle is turning with the calculated radius and the largest value of power recuperation.

The auxiliary clutch is fully disengaged for a period of $t \approx 35$ s - 50 s and then partially engaged to an approximate value of $p \approx 2$ bar.

From $t \approx 50$ s - 80 s, the auxiliary clutch activation pressure is increased to an approximate value of $p \approx 2$ bar, and the vehicle is turning with auxiliary clutch slip because the clutch is partially activated.

From $t \approx 80$ s - 95 s, the driver increases the activation pressure of the auxiliary clutch to the approximate value of $p \approx 4$ bar, resulting in auxiliary clutch slip decrease and thus decreasing the turning radius.

From $t \approx 95$ s - 116 s, the auxiliary clutch is once again fully engaged. The driver then disengages the clutch and ends the turning process.

It is obvious that the curves pS1 and pS1s overlap for almost the entire duration of the analysis because the clutch activation pressure results from the experimental test were used as input parameters for the simulation. This is because the auxiliary clutch activation pressure is the function of the command wheel position, which is an input parameter influenced by the driver.

The high oscillation of the auxiliary clutch pressure pS1 during the time interval $t \approx 35$ s - 50 s comes from the abrupt disengagement process of the auxiliary clutch, which is characterized by large slip losses and unpredictable behavior. Such behavior would cause the simulation to crash, so this transition state is simulated as a continuous process, resulting in large value discrepancies during this time interval.

Experimentally obtained engine angular velocity values-null are interpolated and used as input values for the simulation model IC engine angular velocity-nulls. The measured value represents the driver's throttle demand, making it an input parameter.

The measured angular velocities of the inner and outer tracks are shown in Fig. 18 and labeled n1, n2, while the simulated ones are labeled n1s, n2s, respectively. It is obvious that the simulated output velocities correspond exactly to the character and value of the measured velocities.

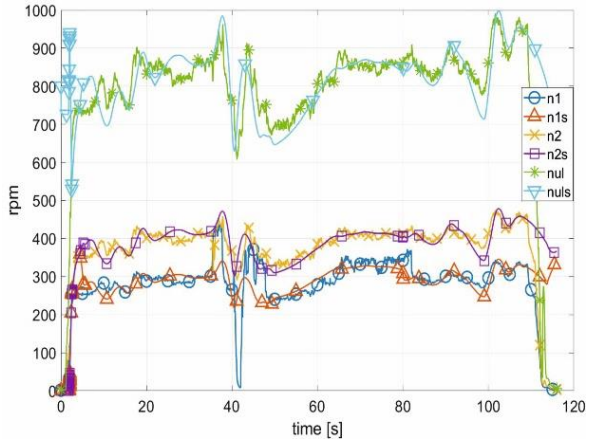

Fig. 18. Input and output rpm-simulation vs experiment.

In the time interval $t \approx 0$ s - 35 s, the inner track velocity has a lower value than the outer track velocity, because the turning mechanism reduces its rotation speed. When the clutch activation pressure drops during the time interval $t \approx 50$ s - 80 s, the inner track velocity increases because the auxiliary clutch is partially activated, resulting in an increase of the turning radius. In the time interval $t \approx 80$ s - 110 s, the auxiliary clutch activation pressure is increased, so the inner track velocity decreases again and the vehicle turns with a lower calculated radius.

A comparison of the measured and simulated torque on the powertrain output shafts is shown in Fig. 19. Curves M2 and M1 represent the measured torque on the outer and inner tracks, respectively, while curves M2s and M1s represent the simulated torque on the outer and inner tracks, respectively.

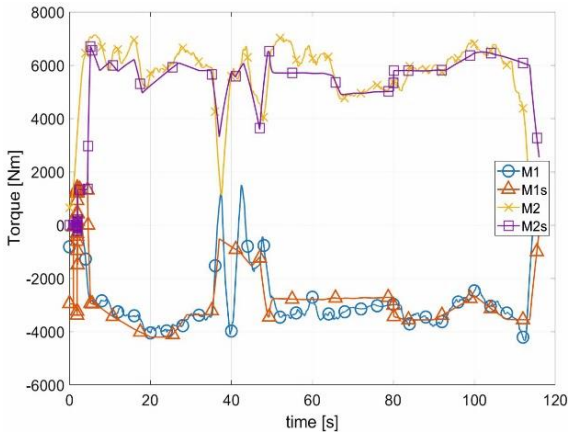

Fig. 19. Inner and outer track torque-simulation vs experiment.

During the time interval t ≈ 0 s - 35 s of the turning process, with the auxiliary clutch fully engaged, both measured and simulated torques have a relatively constant value and a high overlap rate. Negative torque values represent the braking torque on the inner track. Torque oscillations on both inner and outer tracks come from input rpm oscillations.

When the clutch activation pressure decreases in the time interval t ≈ 50 s - 80 s, the clutch is partially engaged and the vehicle turns with a larger turning radius. With turning radius increase, the turning resistance drops, which explains the torque drop for both simulation and experimental data on both tracks.

During the time interval t ≈ 80 s - 110 s, the auxiliary clutch is fully engaged again, the turning radius drops, so the turning resistance increases, thus increasing the torque.

Matching the power balance curves of the simulation with the experimental ones is of great importance for the assessment of the powertrain efficiency. The power delivered to the inner and outer tracks is shown in Fig. 20.

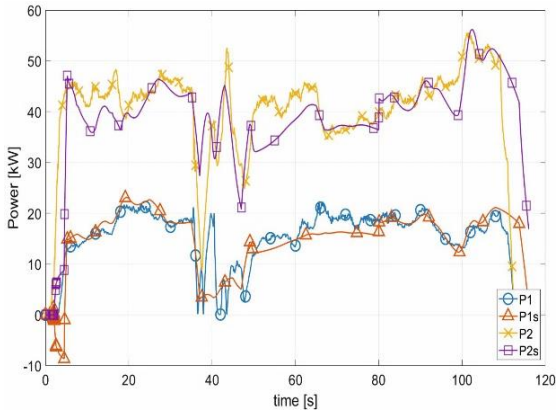

Fig. 20. Inner and outer track power-simulation vs experiment.

Curves P1 and P2 represent the experimental values of power delivered to the inner and outer tracks, respectively, while curves P1s and P2s represent the same physical values in the simulation model. The power results for both experiment and simulation are calculated from dynamic and kinematic values.

During the time interval t ≈ 0 s - 35 s of the turning process, turning with the auxiliary clutch fully engaged is relatively stable from a power balance point of view in both the simulation and the experiment. During the time interval t ≈ 50 s-80 s, the auxiliary clutch is partially engaged, resulting in increased power loss due to slip. This power loss is observed on the outer track because the power delivered on the outer track depends on the ICE power, the power delivered on the inner track, and the power lost due to clutch slip [31]. This can be concluded from (11)

$$P_2 = P_{mz} \cdot \eta_t + P_1 \cdot \eta_p - P_s \cdot \eta_t \qquad (11)$$

where

- P_2, P_1 - power delivered on the outer and inner track
- P_{mz} - IC engine power required for the turning process
- P_s - power lost due to auxiliary clutch slip
- η_t, η_p - losses in powertrain mechanical components

It is obvious that the greater the losses due to clutch slip, the less power is delivered to the outer track. This can be seen in Fig. 20.

From t ≈ 65 s to the end of the simulation, the power curve changes as expected; as the clutch slip decreases, the power delivered is greater and vice versa.

4. DISCUSSION

The time frame of t ≈ 35 s - 50 s is not considered for the comparison and analysis of the experimental test and simulation data. The clutch transition states are a stochastic process that is difficult to predict and simulate. The main goal is to prove the consistency of the experimental and simulation results during the steady states.

To assess the accuracy of the simulation model, the relative errors of the simulated results compared to the experimental results are calculated and displayed. The relative errors are calculated for the entire experiment/simulation time interval, excluding the abrupt auxiliary clutch transition state at t ≈ 35 s - 50 s.

The relative errors of the output angular velocity are shown in Fig. 21. The average value of the relative rpm error on the outer track is about 4%, while on the inner track it is about 6%. For most of the analyzed interval, when the vehicle is moving in stable regimes, the relative error is even lower. The maximum values of the relative rpm errors are in the range where the auxiliary clutch is partially engaged and slipping at t ≈ 50 s - 80 s, which is an unpredictable behavior that was difficult to simulate and will be part of further research. The input rpm oscillation at t ≈ 50 s has a low impact on the rpm output values, having a greater impact on the consistency of the experimental and simulation data for torque and power. Even with this taken into account, the relative errors are acceptable and the simulation rpm curves follow the change character of the experimental rpm results, showing the high accuracy of the simulation model kinematics.

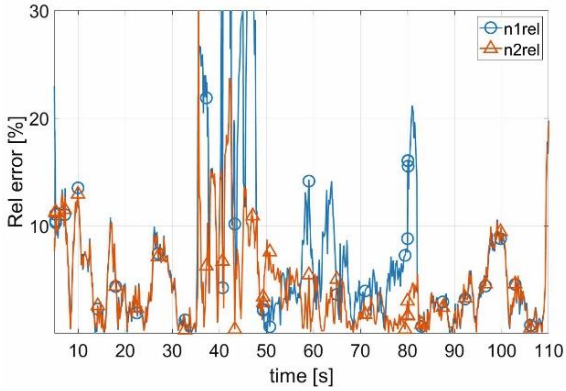

Fig. 21. RPM relative error-simulation vs experiment.

The relative errors of the simulated output torque compared to the measured output torque are shown in Fig. 22.

For the time intervals t ≈ 0 s - 35 s and t ≈ 80 s - 110 s, when the auxiliary clutch is fully engaged, the average value of the relative torque error is about 5.5% on the outer track and 8% on the inner track. The average value of the relative torque error during the auxiliary clutch partial engagement and slip at t ≈ 50 s - 80 s is about 7% on the outer track and 13% on the inner track. It is evident that in the regimes where

the auxiliary clutch is fully engaged, which are relevant for the simulation model accuracy assessment, the relative errors are lower. The average relative error values during the auxiliary clutch slip, although higher, are also acceptable. The torque decrease at t ≈ 50 s occurs with some delay due to the significant input rpm drop, especially on the outer track, where a change in adhesion conditions was observed, resulting in a delayed resistance decrease, which is why the difference between the measured and simulated torque is higher. For the whole analyzed range, the simulated torque curves follow the change character of the experimental result curves, which proves the validity of the simulation model dynamics.

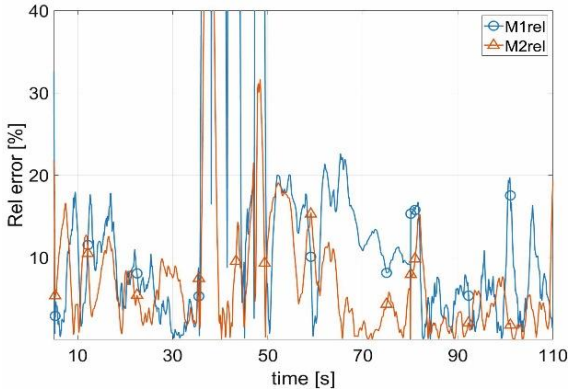

Fig. 22. Torque relative error-simulation vs experiment.

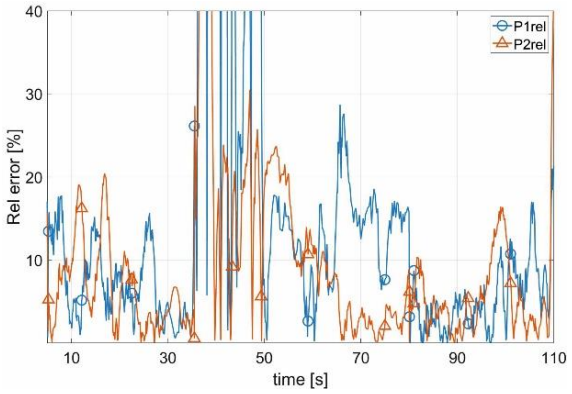

Fig. 23. Power relative error-simulation vs experiment.

The relative errors of the simulated output power compared to the experimental output power are shown in Fig. 23. Since power is a value derived from torque and angular velocity, it is obvious that the relative power error curves have the same characteristic points as the relative torque and rpm error curves for the same reasons. For the time intervals t ≈ 0 s - 35 s and t ≈ 80 s - 110 s, when the auxiliary clutch is fully engaged, the average value of the relative power error is about 6.5% on the outer track and 7% on the inner track. The average value of the relative power error during the auxiliary clutch partial engagement and slip at t ≈ 50 s - 80 s is about 8% on the outer track and 13% on the inner track. Although the relative errors are higher during the auxiliary clutch slip, the average value of the relative power error is acceptable for both auxiliary clutch states. Given the fact that the simulation power curves follow the character of the experimental power curves, it is evident that the simulation model is credible with the real model in both kinematic and dynamic parameters.

5. Conclusion

The validation of the simulation model of the subject vehicle is of great importance, as it allows to run various tests of vehicle movement and powertrain behavior with a high accuracy rate compared to the experimental tests.

Another significant contribution of the developed model is that it can be easily adapted and applied to numerous tracked vehicles with mechanical turning mechanisms, completely changing and improving their design.

It is important that the significant parameters of the simulation model correspond to the measured physical quantities during the relevant part of the test when the auxiliary clutch was fully engaged (steady states). On average, the simulated kinematic values deviate from the experimental values by 4% to 6%, which the authors consider acceptable. The simulated dynamic values deviate from the experimental values by 5% to 8%, which is also considered acceptable by the authors of this paper.

Regimes where the vehicle was moving with the auxiliary clutch partially engaged show slightly higher experiment-simulation data discrepancies (7%-13%). The authors intend to further develop the simulation model to perform more accurate simulations of friction element slip and transition processes and analyze their effects on the power recuperation process. In addition, the simulation model will be used for the modernization of vehicles with hybrid drive systems, so that the verified simulation model will serve as a reference for the modernized vehicle model.

References

[1] Ryu, H., Bae, D., Choi, J., Shabana, A. A. (2000). A compliant track link model for high-speed, high-mobility tracked vehicles. *International Journal for Numerical Methods in Engineering*, 48, 1481-1502. https://doi.org/10.1002/1097-0207(20000810)48:10%3C1481::AID-NME959%3E3.0.CO;2-P

[2] Castellazzi, L., Tonoli, A., Amati, N., Galliera, E. (2017). A study on the role of powertrain system dynamics on vehicle driveability. *Vehicle System Dynamics*, 55 (7), 1012-1028. https://doi.org/10.1080/00423114.2017.1294699

[3] Wong, J. Y., Preston-Thomas, J. (1986). Parametric analysis of tracked vehicle performance using an advanced computer simulation model. *Proceedings of the Institution of Mechanical Engineers, Part D: Transport Engineering*, 200 (2), 101-114. https://doi.org/10.1243/PIME_PROC_1986_200_170_02

[4] Wong, J. Y. (1986). Computer aided analysis of the effects of design parameters on the performance of tracked vehicles. *Journal of Terramechanics*, 23 (2), 95-124. https://doi.org/10.1016/0022-4898(86)90017-0

[5] Adegbohun, F., von Jouanne, A., Phillips, B., Agamloh, E., Yokochi, A. (2021). High performance electric vehicle powertrain modeling, simulation and validation. *Energies*, 14 (5), 1943. https://doi.org/10.3390/en14051493

[6] Dalsjø, P. (2008). *Hybrid electric propulsion for military vehicles - overview and status of the technology*. FFI Report 2008/01220, Norwegian Defence Research Establishment (FFI), Kjeller, Norway. ISBN 978-82-464-1394-5.

[7] Dhir, A., Sankar, S. (1995). Assessment of tracked vehicle suspension system using a validated computer simulation model. *Journal of Terramechanics*, 32 (3), 127-149. https://doi.org/10.1016/0022-4898(95)00012-7

[8] Yi, K. S., Yi, S.-J. (2005). Real-time simulation of a high speed multibody tracked vehicle. *International Journal of Automotive Technology*, 6 (4), 351-357.

[9] MATLAB. (2018). *version 9.7.0.1190202 (R2019b)*. The MathWorks Inc., Natick, Massachusetts.

[10] Janarthanan, B., Padmanabhan, C., Sujatha, C. (2012). Longitudinal dynamics of a tracked vehicle: Simulation and experiment. *Journal of Terramechanics*, 49 (2), 63-72. https://doi.org/10.1016/j.jterra.2011.11.001

[11] Kiyakli, A. O., Solmaz, H. (2018). Modeling of an electric vehicle with MATLAB/Simulink. *International Journal of Automotive Science and Technology*, 2 (4), 9-15. https://doi.org/10.30939/ijastech..475477

[12] Nabaglo, T., Kowal, J., Jurkiewicz, A. (2013). Construction of a parametrized tracked vehicle model and its simulation in MSC.ADAMS program. *Journal of Low Frequency Noise, Vibration and Active Control*, 32 (1-2), 167-173. https://doi.org/10.1260/0263-0923.32.1-2.167

[13] Kciuk, S., Mezyk, A. (2010). Modelling of tracked vehicle dynamics. *Journal of Kones*, 17 (1), 223-232.

[14] Madsen, J., Heyn, T., Negrut, D. (2018). *Methods for tracked vehicle system modeling and simulation*. Technical Report 2010-01.

[15] Blundell, M., Harty, D. (2004). Introduction. In *The Multibody Systems Approach to Vehicle Dynamics.* Butterworth-Heinemann, 1-22. ISBN 9780080473529.

[16] Yi, T. (2000). Vehicle dynamic simulations based on flexible and rigid multibody models. In *SAE 2000 World Congress*. https://doi.org/10.4271/2000-01-0114

[17] Balamurugan, S., Srinivasan, R. (2017). Tracked vehicle performance evaluation using multi body dynamics. *Defence Science Journal*, 67 (4), 476-480. https://doi.org/10.14429/dsj.67.11534

[18] Hryciów, Z., Rybak, P. (2019). Numerical research of the high-speed military vehicle track. *AIP Conference Proceedings*, 2078 (1), 020029. https://doi.org/10.1063/1.5092032

[19] Mahalingam, I., Padmanabhan, C. (2021). A novel alternate multibody model for the longitudinal and ride dynamics of a tracked vehicle. *Vehicle System Dynamics*, 59 (3), 433-457. https://doi.org/10.1080/00423114.2019.1693048

[20] Taratorkin, I., Derzhanskii, V., Taratorkin, A. (2016). Experimental determination of kinematic and power parameters at the tracked vehicle turning. *Procedia Engineering*, 150, 1368-1377. https://doi.org/10.1016/j.proeng.2016.07.331

[21] Zhang, Y., Qiu, M., Liu, X., Li, J., Song, H., Zhai, Y., Hu, H. (2021). Research on characteristics of tracked vehicle steering on slope. *Mathematical Problems in Engineering*, 2021, 3592902. https://doi.org/10.1155/2021/3592902

[22] Ogorkiewicz, R. (1991). *Technology of Tanks*. Jane's Information Group, ISBN 978-0710605955.

[23] Muždeka, S. (2012). *Osnovi borbenih vozila: udžbenik*. Beograd, Serbia: Medija centar Odbrana, ISBN 9788633503693. (in Serbian)

[24] Ponorac, L., Grkić, A., Muždeka, S. (2021). Hybrid power trains for high-speed tracked vehicles. *Mobility and Vehicle Mechanics*, 47 (3), 35-48. https://doi.org/10.24874/mvm.2021.47.03.04

[25] Muždeka, S., Perić, S. (2012). *Osnovi borbenih vozila: praktikum za vežbe*. Beograd, Serbia: Medija centar Odbrana, ISBN 9788633503761. (in Serbian)

[26] Guo, T., Guo, J., Huang, B., Peng, H. (2019). Power consumption of tracked and wheeled small mobile robots on deformable terrains-model and experimental validation. *Mechanism and Machine Theory*, 133, 347-364. https://doi.org/10.1016/j.mechmachtheory.2018.12.001

[27] Stojkovic, V., Mikulic, D. (2002). The impact of a fixed kinematic turning radius of a tracked vehicle on the engine power required in a turn. *Strojniski Vestnik - Journal of Mechanical Engineering*, 48, 459-466.

[28] Vesic, M., Muzdeka, S. (2007). Analysis of influence of turning system kinematic scheme on turning power balance for high speed tracked vehicles. *Vojnotehnicki Glasnik*, 55 (2), 149-168. https://doi.org/10.5937/vojtehg0702149V

[29] Jimenez-Espadafor, F. J., Becerra Villanueva, J. A., Palomo Guerrero, D., Torres García, M., Carvajal Trujillo, E., Fernández Vacas, F. (2014). Measurement and analysis of instantaneous torque and angular velocity variations of a low speed two stroke diesel engine. *Mechanical Systems and Signal Processing*, 49 (1), 135-153. https://doi.org/10.1016/j.ymssp.2014.04.016

[30] Chen, C., Ma, T., Jin, H., Wu, Y., Hou, Z., Li, F. (2020). Torque and rotational speed sensor based on resistance and capacitive grating for rotational shaft of mechanical systems. *Mechanical Systems and Signal Processing*, 142, 106737. https://doi.org/10.1016/j.ymssp.2020.106737

[31] Ponorac L., Blagojević, I., Grkić, A. (2022). Analysis of powertrain's workload during the turning process of a high-speed tracked vehicle. *IOP Conference Series: Materials Science and Engineering*, 1271, 12003. https://doi.org/10.1088/1757-899X/1271/1/012003

Accepted September 18, 2023
Received May 15, 2023